Photodissociation of IO (355 nm) and OIO (532 nm): Quantum Yields for $O(^3P)$ and $I(^2P_J)$ Production

Trevor Ingham, Melanie Cameron, and John N. Crowley*

Max-Planck-Institut für Chemie, Division of Atmospheric Chemistry, Postfach 3060, 55020 Mainz, Germany

Received: March 28, 2000; In Final Form: June 15, 2000

The photodissociation of IO and OIO was investigated using 2-color, pulsed laser photolytic generation and dissociation of these species, combined with the detection of product atoms by resonance fluorescence. IO radicals were generated in the reactions of $O(^3P)$ with I_2, $O(^3P)$ with CF_3I, and $I(^2P_J)$ with O_3 and were detected by absorption spectroscopy. The self-reaction of IO was used as the source of OIO, which was also detected by absorption spectroscopy. The quantum yield of $O(^3P)$ formation following the photolysis of IO at 355 nm was measured relative to NO_2 photolysis at the same wavelength and was found to be $0.91 \pm {}^{0.19}_{0.26}$. $O(^3P)$ was not detected in the photolysis of OIO at 532 nm, enabling us to place an upper limit to the quantum yield of 7×10^{-3} at this wavelength. $I(^2P_J)$was detected in the 532-nm photolysis of OIO but was formed only at very high laser fluence, presumably in a sequential two-photon process. These results show that OIO is probably stable with respect to photolysis in its strong visible absorption band between ≈480 and 660 nm, which has important implications for the iodine chemistry of the marine boundary layer.

1. Introduction

Recent measurements of photolabile iodocarbons at concentrations close to several parts per trillion by volume (pptv) in the marine boundary layer have led to a reassessment[1] of the role of iodine compounds in tropospheric chemistry, which has been a subject of debate for approximately two decades.[2−6] Biogenic iodocarbons produced by marine algae are the major source of iodine in the atmosphere.[2] The production of reactive iodine from these compounds occurs mainly via photodissociation, with lifetimes varying from 200 s to 90 h,[7] to yield iodine atoms, $I(^2P_J)$, which subsequently react with ozone to form the iodine oxide radical, IO:

$$I + O_3 \rightarrow IO + O_2 \quad (1)$$

Recent field measurements in the marine boundary layer (MBL) at Mace Head, Ireland, indicated peak IO mixing ratios of greater than 6 pptv,[8] which were correlated with the presence of iodocarbons such as, CH_3I, CH_2I_2, and C_2H_5I.[9]

Major loss processes of the IO radical are photolysis, reaction with HO_2, and, in more polluted environments, reaction with NO and NO_2:

$$IO + h\nu \rightarrow O(^3P) + I \quad (2)$$

$$IO + HO_2 \rightarrow HOI + O_2 \quad (3)$$

$$IO + NO \rightarrow NO_2 + I \quad (4)$$

$$IO + NO_2 + M \rightarrow IONO_2 + M \quad (5)$$

Both HOI[10] and $IONO_2$ have strong absorption spectra in the actinic region and are rapidly photolyzed to return $I(^2P_J)$ or IO back to the gas phase, and they cannot be considered efficient daytime reservoirs of iodine:

$$HOI + h\nu \rightarrow OH + I \quad (6)$$

$$IONO_2 + h\nu \rightarrow I + NO_3 \quad (7a)$$

$$\rightarrow IO + NO_2 \quad (7b)$$

When sufficient IO is present and the amount of NO*x* (NO*x* = NO_2 + NO) is low, the self-reaction can be an important loss process:

$$IO + IO \rightarrow I + OIO \quad (8a)$$

$$\rightarrow I_2 + O_2 \quad (8b)$$

$$\rightarrow 2I + O_2 \quad (8c)$$

$$IO + IO + M \rightarrow I_2O_2 + M \quad (8d)$$

Recent studies of reaction 8[11,12] have observed iodine dioxide, OIO, as a major product. This result is consistent with the observation of both IO and its self-reaction product OIO in the MBL at Mace Head, Ireland, when the amount of NO*x* is low.[8]

Modeling studies,[13,14] field experiments,[15] and laboratory investigations[16] have revealed the potential for bromine activation by catalytic reactions on aqueous sea-spray, with predicted daytime BrO mixing ratios of ≈0.5−5 pptv in the remote marine boundary layer. At these concentrations, BrO can be an important reaction partner for IO. Recent studies of this reaction have identified OIO as a major product[12,17] with a branching ratio between 0.65 and 1.0 for the reaction channel that produces OIO and Br atoms:[17]

$$IO + BrO \rightarrow Br + OIO \quad (9)$$

Both laboratory experiments and field measurements have thus identified OIO as a potentially important iodine reservoir

* To whom correspondence should be addressed.

10.1021/jp001166p CCC: $19.00
Published on Web 08/05/2000

in the troposphere.[12] As with HOI and $IONO_2$, the efficiency as an iodine reservoir will depend on its stability with respect to photolysis. The gas-phase absorption spectrum of OIO was first characterized by Himmelmann et al.,[11] who attributed a transient, structured absorption in the visible region between 480 and 660 nm to OIO. In later work, absorption cross sections of $\approx 1 \times 10^{-17}$ cm^2 at 548.6 nm[12] and $(2-5) \times 10^{-17}$ cm^2 at 549.1 nm were determined.[18] An absorption cross section of this magnitude in the visible region of the spectrum will result in an exceedingly short lifetime with respect to photodissociation, if the absorption is dissociative.

To date, there are no experimental studies of the photophysical processes following absorption of a photon in the visible absorption band of OIO. However, ab initio calculations[19] have predicted a relatively high thermochemical stability for OIO, with $\Delta H_f(298)\text{OIO} = 76.7 \pm 15$ kJ mol^{-1}. This results in a bond dissociation energy for OI−O of 288 ± 16 kJ mol^{-1} and a thermodynamic photodissociation threshold of 414 ± 23 nm for reaction 10a (the uncertainty reflects the conservative error limit set by $\Delta H_f(298)$OIO (above) and the error limit for $\Delta H_f(298)\text{IO} = 115.9 \pm 5.0$ kJ mol^{-1}):[20]

$$\text{OIO}\ (^2\text{B}) + h\nu \rightarrow \text{IO}\ (^2\Pi) + \text{O}(^3\text{P}) \qquad (10a)$$

The long-wavelength cutoff (437 nm) of the calculated photodissociation threshold for O(^{3}P) and IO formation occurs at a significantly shorter wavelength than the observed absorption due to OIO between 480 and 660 nm, which indicates that OIO, in stark contrast to HOI and $IONO_2$, may be stable with respect to photolysis (at least in the visible band) and may well be the most photochemically stable of the major iodine reservoir species.[12]

The aim of the present study was to provide the missing quantum yield data for the photolysis of OIO in its visible absorption bands that, in combination with the absorption cross section, enables its true atmospheric photolysis rate to be determined. As part of the study, we also determined for the first time the quantum yields of photolysis of IO at 355 nm in its continuum region of absorption, which to date has been assumed to be unity but has remained unconfirmed by direct experimental study.

2. Experimental Section

The pulsed laser photolysis/UV−visible absorption/resonance fluorescence (RF) apparatus used in this work has been described elsewhere,[10,21,22] and only details relevant to the present study are given here. All experiments were performed at 295 ± 2 K in 60 Torr N_2 as bath gas.

A 1.25-m long cylindrical cell of 5-cm internal diameter equipped with quartz end windows was used as the reaction/absorption/RF cell (Figure 1). Dielectric mirrors enabled the photolysis beams from an excimer laser (248 or 351 nm, 20-ns pulse width) and a Nd:YAG laser, (second harmonic at 532 nm or third harmonic at 355 nm, 6-ns pulse width) and the analysis light (Halogen lamp, D_2 lamp) to be overlapped collinearly along the cell's major axis. In some experiments, a continuous-wave, intra-cavity frequency-doubled Nd:YAG laser (CW-2ω Nd:YAG) was also used as an analysis light source. The two pulsed photolysis beams were apertured down to a diameter of approximately 4 mm so that they were slightly larger than the diameter of the resonance lamp emission at the point of intersection. With the flow conditions employed (see below), it was possible to run both lasers at 10 Hz, so that the photolyzed volume between the cell entrance window and the RF detection

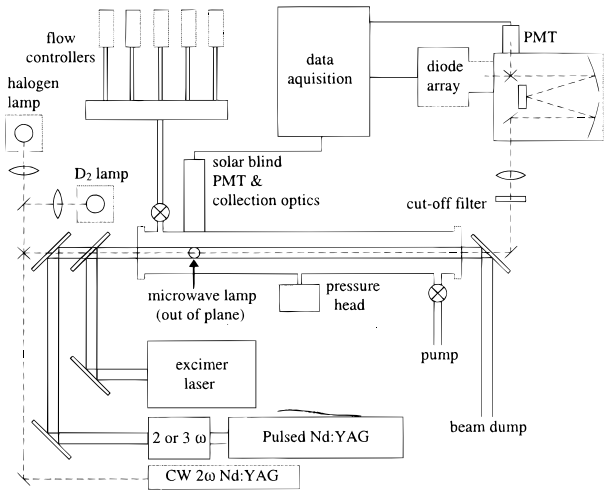

Figure 1. Schematic diagram of the experimental setup.

zone was replenished with fresh reactants prior to the next laser pulse. The synchronization of the lasers was controlled by a commercial delay generator, and the fluence was measured by use of a calibrated Joule meter.

The analysis light, which sampled only the volume swept out by the apertured laser beams, was detected by a monochromator (0.5 m, grating with 300 lines mm^{-1}) equipped with both an intensified, gated diode array and a photomultiplier tube. The spectral resolution for the diode array measurements was approximately 0.7 nm; the wavelength axis was calibrated to an accuracy of 0.3 nm using the emission lines of a Hg Pen-Ray lamp. For the time-resolved absorption measurements of IO and OIO, a resolution of 0.16 nm was used, as determined by measuring the bandwidth of an isolated Hg atomic line. The line width of the CW Nd:YAG laser was much narrower than our instrument resolution. I_o was obtained by averaging the PMT signal obtained shortly before the laser pulse, and I_t values were recorded after the laser pulse. The absorption was calculated by use of the relationship $\text{Abs}_t = \ln(I_o/I_t)$.

The two orthogonal RF axes for excitation and collection were situated approximately 10 cm from the entrance to the cell and were orthogonal to the photolysis axis. The atomic resonance lamp used to excite resonance fluorescence in photolytically generated O(^{3}P) consisted of an electrode-less microwave discharge through a flow of about 3 Torr He. The total lamp pressure was adjusted to obtain the optimum signal-to-noise ratio. The lamp emission passed through a calcium fluoride filter and through a series of baffles flushed with N_2. The calcium fluoride filter prevented Lyman-α radiation from entering the cell but transmitted the O(^{3}P) line around 130 nm. For the detection of I, an additional flow of I_2 highly diluted in He was added to the lamp, which was run at a total pressure of 3 Torr. The baffles were flushed with N_2O or C_2H_6 ($\approx$400 Torr cm) to prevent the simultaneous detection of O(^{3}P). A small flow of O_2 was added to the reactor to quench any electronically excited I atoms I(^{2}P$_{1/2}$) rapidly to the ground-state I(^{2}P$_{3/2}$).[23,24] With this setup, we therefore detect both spin−orbit states, I(^{2}P$_J$) as I(^{2}P$_{3/2}$).

Resonance fluorescence from O(^{3}P) or I(^{2}P$_J$) was collected via a magnesium fluoride lens (orthogonal to the excitation and laser axes) and was directed to the front plate of a solar blind PMT (CsI photocathode). The signals were processed by use of photon counting techniques in conjunction with multichannel scaling. The detection limit for O(^{3}P) was determined by photolyzing a known concentration of NO_2 ($5-50 \times 10^{13}$ cm^{-3})

at 355 nm with a known laser fluence (8−30 mJ cm^{-2}) to generate a known concentration of $O(^3P)$:

$$NO_2 + h\nu\ (355\ nm) \rightarrow O(^3P) + NO \qquad (11)$$

The detection limit for $O(^3P)$ was found to be approximately 5×10^9 cm^{-3} for $O(^3P)$ (in 60 Torr N_2) for an integration time of 50 ms. For $I(^2P_J)$, we determined the detection limit by photolyzing CH_2I_2 in a large excess of O_3 and monitoring both the $I(^2P_J)$ decay and the IO absorption profile in back-to-back experiments. The IO absorption could then be converted to an absolute concentration using literature cross sections at the monitoring wavelength and the initial $I(^2P_J)$ concentration extracted by analysis of the formation and decay kinetics of IO. The detection limit for $I(^2P_J)$ was found to be $\approx (2-3) \times 10^9$ cm^{-3} for 80-ms integration time.

2.1. Chemicals and Gas-Handling. Ozone was prepared using a commercial ozonizer and was stored on silica gel at −78 °C. It was admitted to the cell by passing a regulated flow of N_2 through the storage trap, the temperature of which could be varied between −40 and −78 °C. A flow of I_2 was generated by passing N_2 through a U-tube containing I_2 at ambient temperature. CF_3I was added directly via a flow controller. Dilute mixtures of NO_2 in N_2 were prepared and admitted via a flow controller. The concentration of the reactants were determined in situ by diode array absorption using literature spectra of O_3,[25] CF_3I,[25] NO_2,[26] CH_2I_2,[7] and I_2.[27] The stated purities of the chemicals used were as follows: I_2 (99.8%, Aldrich), CF_3I (99%, Aldrich), NO_2 (99.5%, Union Carbide), CH_2I_2 (99%, Aldrich), He (99.996%, Linde), and N_2 (99.996%, Aldrich). I_2 was re-distilled prior to; NO_2 and CF_3I were used without further purification.

3. Results and Discussion

3.1. Formation and Self-Reaction of IO. In these experiments, IO was generated by the 248-nm (20−60 mJ cm^{-2}) photolysis of O_3 ($5-20 \times 10^{12}$ cm^{-3}) in the presence of excess I_2 ($5-50 \times 10^{13}$ cm^{-3}) in 60 Torr N_2, as shown by reactions 12−14. The bath gas ensured that $O(^1D)$ formed in the photolysis was relaxed to $O(^3P)$ in < 20 ns via reaction 13, which is effectively instantaneous relative to the subsequent chemistry:

$$O_3 + h\nu\ (248\ nm) \rightarrow O(^3P) + O_2 \qquad (12a)$$

$$\rightarrow O(^1D) + O_2 \qquad (12b)$$

$$O(^1D) + N_2 \rightarrow O(^3P) + N_2 \qquad (13)$$

$$O(^3P) + I_2 \rightarrow IO + I \qquad (14)$$

With total a pressure of 60 Torr and a flow rate of 10 L (STD) min^{-1} (slm), the total residence time in the cell was about 1 s. For time-resolved absorption measurements of IO, and OIO, the time between the laser pulses was always greater than the total residence time to ensure that the reaction products were removed prior to the next pulse. Time-resolved absorption profiles of the IO radical were measured at 427.2 nm and converted to concentration profiles by use of the absorption cross section ($(3.6 \pm 0.5) \times 10^{-17}$ cm^2) given by Harwood et al.[28]

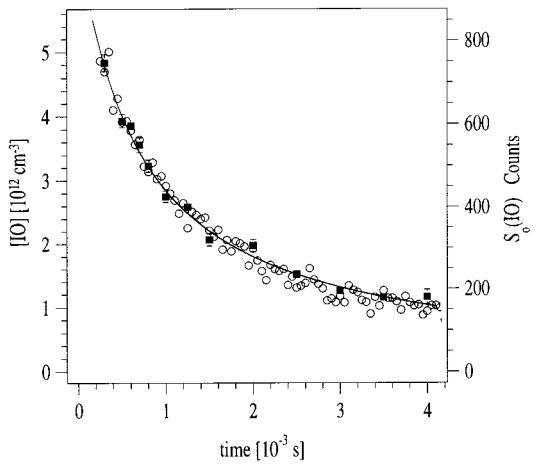

Figure 2. A comparison between the IO decay measured both by absorption spectroscopy and photofragment spectroscopy. The ordinate on the left refers to absorption (open circles) and that on the right to RF (filled squares). The error bars on the RF data points are 2σ from the back extrapolation of fits to the $O(^3P)$ decays to get S_o. The solid line is a fit to the absorption decay and lies on top of the fit to the S_o(IO) data. The initial [IO] was 6×10^{12} cm^{-3}; 355-nm laser fluence $\approx$ 30 mJ cm^{-2}. The absorption time resolution was 50 μs per channel, and the RF decays were obtained from 1000 laser pulses to give a total integration time of 20 ms per channel.

The instrument resolution employed in the present study was similar to that used by these authors. Typically, the initial [IO] was maintained at or below 5×10^{12} cm^{-3} to avoid the potential problems associated with aerosol formation with this source chemistry. A typical IO decay measured in this manner is presented in Figure 2. The IO decays were analyzed with the equation:

$$1/[IO]_t = 1/[IO]_0 + 2k_8 t \qquad (i)$$

where $[IO]_0$ is the initial IO concentration and $[IO]_t$ the IO concentration at time = t after the 248-nm laser pulse. Analysis of approximately twenty IO decays yielded a value of $k_8 = (9.0 \pm 1.7) \times 10^{-11}$ cm^3 s^{-1}, which is in good agreement with the current recommendation. The quoted uncertainty refers to statistical scatter at the 2σ level and the 14% systematic error in $\sigma_{427.2\ nm}$(IO).[28] This value was independent of initial [IO] ((3−6) $\times 10^{12}$ cm^{-3}) and also shows no evidence for the reformation of IO in the reaction of $I(^2P_J)$ with O_3, as, at the laser fluences and O_3 concentrations used, most of the O_3 was removed by photolysis.

3.2. Photolysis of IO at 355 nm; Quantum Yield for $O(^3P)$ Formation. The IO quantum yield experiments were performed relative to NO_2 in a back-to-back fashion. First, the [IO]−time profile was measured as described above with time-resolved absorption spectroscopy using only the excimer laser at 248 nm (≈30−60 mJ cm^{-2}; repetition rate 0.8 Hz). Second, under the same experimental conditions and laser fluence, experiments were carried out in which the 355-nm laser was triggered at a set delay after the 248-nm laser (both lasers operating at 10 Hz), and $O(^3P)$ profiles were monitored by RF. Typical raw data is shown in Figure 3, which shows the exponential decay of the primary $O(^3P)$ formed at $t = 0$ in reactions 12 and 13 and lost in reaction 14. The rate of decay of $O(^3P)$ is consistent with reaction with 6×10^{13} cm^{-3} I_2 and the rate coefficient at room temperature ($k_{14} = 1.4 \times 10^{-10}$ cm^3 s^{-1}).

After 1.5 ms, once the IO has decayed to ≈2.5 ‰ of its initial concentration, the 355-nm laser is triggered and the secondary $O(^3P)$ signal from the photolysis of IO at 355 nm was monitored.

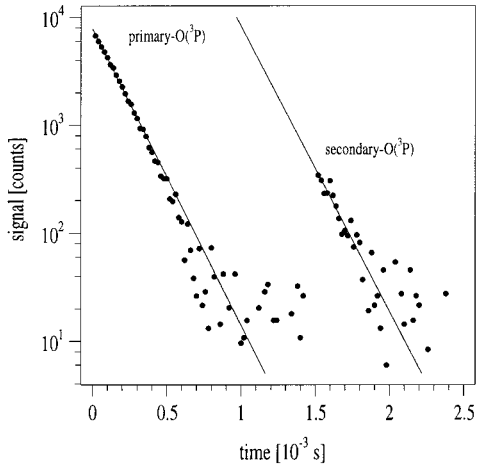

Figure 3. An example of an IO photolysis experiment. The decay of primary $O(^3P)$ from the 248-nm photolysis of O_3 due to reaction with I_2 was followed to completion; then, the 355-nm laser was triggered 1.5 ms after the excimer laser to produce secondary $O(^3P)$ from the photolysis of IO. Initial $[IO] = 5 \times 10^{12}$ cm^{-3}, and [IO] at $t = 1.5$ ms was 2.0×10^{12} cm^{-3}. The 248- and 355-nm laser fluences were ≈60 and 30 mJ cm^{-2}, respectively, and the decays were obtained from 1000 laser pulses to give a total integration time of 20 ms per channel. The solid lines are exponential fits to the decays.

This was extrapolated back to exactly $t = 1.5$ ms to obtain $S_o(IO)$:

$$\text{primary } O(^3P) + I_2 \rightarrow IO + I \qquad (14)$$

$$IO + h\nu \rightarrow \text{secondary } O(^3P) + I \qquad (15)$$

Perturbation to the secondary $O(^3P)$ signal due to O_3 photolysis at 355 nm in the absence of I_2 was not observed, which is consistent with the small absorption cross section of O_3 at this wavelength ($\approx 1 \times 10^{-22}$ cm^2) [25] and its low concentration. To confirm that the secondary $O(^3P)$ signal originated from IO, the time between the 248- and 355-nm laser pulses was varied to cover the entire IO decay. The results of this are given in Figure 2, which shows a comparison between the IO decay measured with absorption spectroscopy and that obtained by photolysis and $O(^3P)$ detection. The $S_o(IO)$ data has been scaled to match the [IO]−time profile. The good agreement between the shape of the two profiles clearly demonstrates that the origin of secondary $O(^3P)$ is the photolysis of IO and that there is no observable interference in the RF measurements from 355-nm photolysis of products of the IO self-reaction (e.g., OIO or possibly IOOI).

A correction to the $O(^3P)$ signals was made to account for the attenuation of fluorescence by the I_2 present. With $[O_3] \approx 5 \times 10^{12}$ cm^{-3}, $[I_2] = (0-1) \times 10^{14}$ cm^{-3}, and a 248-nm fluence of ≈30 mJ cm^{-2}, $O(^3P)$ profiles were obtained and extrapolated to zero time to obtain $S_o(O_3)$. Figure 4 shows a plot of $S_o(O_3)$ versus $[I_2]$. With the extent of fluorescence attenuation by I_2 established, it was possible to correct the $S_o(IO)$ obtained in the quantum yield measurements.

We note that if the initial [IO] was increased above $\approx 1 \times 10^{13}$ cm^{-3}, an increase in the RF background signal (after the $O(^3P)$ had decayed) was observed, which was interpreted as scattering of the lamp emission by aerosol formation. If the $[IO]_o$ was increased further, this background signal was observed to increase with time. All quantum yield measurements were performed with the initial [IO] maintained at $\leq 5 \times 10^{12}$ cm^{-3}, where we observed no indication of aerosol formation.

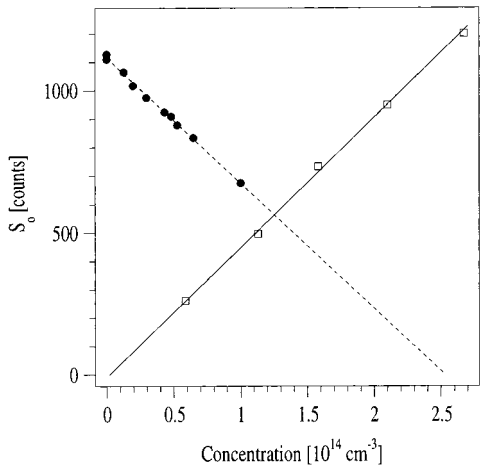

Figure 4. A plot of S_o vs concentration: (i) $S_o(O_3)$ versus $[I_2]$ (filled circles, dashed line fit) shows that there is significant attenuation of the lamp emission and fluorescence signal in the presence of I_2. The error bars representing the 2σ error in $S_o(O_3)$ from the exponential fit to the decays are within the data points. 248-nm laser fluence ≈ 30 mJ cm^{-2}; $[O_3] \approx 3 \times 10^{12}$ cm^{-3}. The $O(^3P)$ decays were obtained from 1000 laser pulses to give a total integration time of 20 ms per channel. These data were used to correct the $S_o(IO)$ in the quantum yield measurements. (ii) $S_o(NO_2)$ versus $[NO_2]$ (open squares, solid line fit) shows the linear relationship, indicating that there is no observable attenuation of the lamp emission or fluorescence signal by NO_2 over this concentration range. 355-nm laser fluence ≈8 mJ cm^{-2}. Error bars and the decays are as (i) above.

Following an IO photofragment experiment, the I_2 and O_3 were replaced by a known concentration of $[NO_2]$ ($5-50 \times 10^{13}$ cm^{-3}), which was then also photolyzed at 355 nm. The $O(^3P)$ signal was extrapolated to zero time to obtain $S_o(NO_2)$, and the 355-nm laser fluence was held constant at ≈8, 20, or 30 mJ cm^{-2}:

$$NO_2 + h\nu\ (355 \text{ nm}) \rightarrow NO + O(^3P) \qquad (11)$$

The decay of the $O(^3P)$ signal is in this case due to reaction with NO_2:

$$O(^3P) + NO_2 \rightarrow O_2 + NO \qquad (16)$$

The pseudo-first-order decay rate of $O(^3P)$ (k') was measured for $[NO_2]$ in the range $5-50 \times 10^{13}$ cm^{-3} to obtain a value of $k_{16} = (1.01 \pm 0.05) \times 10^{-11}$ cm^3 s^{-1}, which is in good agreement with the current recommendation.[25] The quoted uncertainty refers to the combined errors in the weighted fit to the second-order plot and the 4% systematic error in $[NO_2]$. Figure 4 shows the linear relationship between the initial fluorescence signal, $S_o(NO_2)$, and $[NO_2]$ (open squares, solid line fit), which confirms that there is no observable attenuation of the lamp emission or the fluorescence signal by NO_2 under our experimental conditions. Figure 5 shows examples of $O(^3P)$ decays produced both via the photolysis of IO (extrapolated to zero time) and via the photolysis of the reference compound NO_2.

The quantum yield for $O(^3P)$ production in the 355 nm photolysis of IO can be obtained via the relationship (ii):

$$\frac{S_o(IO)_{corr}}{S_o(NO_2)} = \frac{\Phi^{O^3P}_{355\ nm}(IO)\ \sigma_{355\ nm}(IO)\ [IO]}{\Phi^{O^3P}_{355\ nm}(NO_2)\ \sigma_{355\ nm}(NO_2)\ [NO_2]} \qquad \text{(ii)}$$

where $S_o(IO)_{corr}$ and $S_o(NO_2)$ are the initial $O(^3P)$ signals from the photolysis of IO (corrected for attenuation of the fluores-

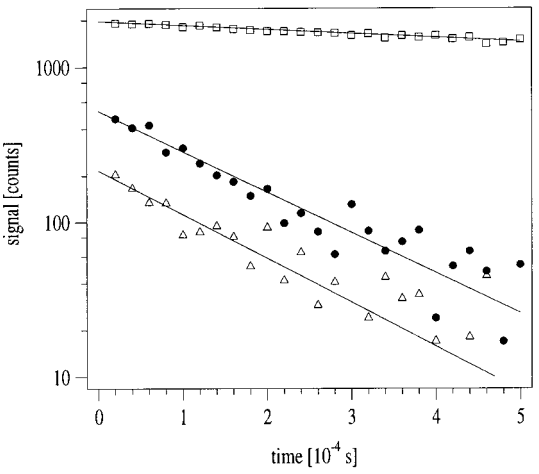

Figure 5. An example of O(^{3}P) decays from the back-to-back photolysis of IO and NO_2 at 355 nm. The square and circular data points refer to the photolysis of 1.05×10^{14} NO_2 and 3.60×10^{12} IO cm^{-3}, respectively, at ≈30 mJ cm^{-2}. The triangles refer to the photolysis of 2.21×10^{12} IO cm^{-3} at ≈20 mJ cm^{-2}. The decays were obtained from 1000 laser pulses to give a total integration time of 20 ms per channel. The solid lines are exponential fits to the decays, which were used to obtain $S_o(NO_2)$ and $S_o(IO)$.

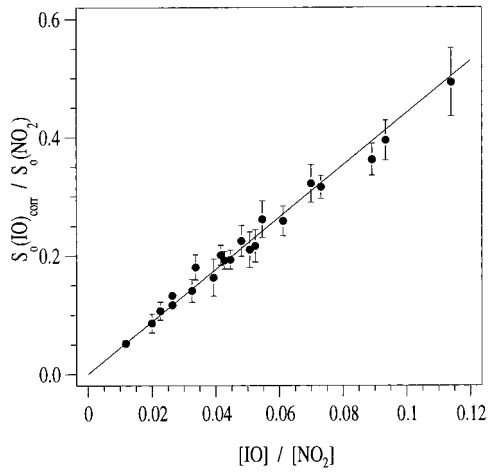

Figure 6. A plot of $S_o(IO)_{corr}/S_o(NO_2)$ versus $[IO]/[NO_2]$, which shows a linear relationship with an intercept close to zero. The error bars shown refer to the relative error (95% confidence level) in $S_o(IO)_{corr}$ and $S_o(NO_2)$ obtained from the back extrapolation of the exponential fits to the respective O(^{3}P) decays. The solid line is a weighted fit to these data, the slope of which gives the quantity $\Phi^{O^3P}_{355\ nm}(IO)\sigma(IO)/\Phi^{O^3P}_{355\ nm}(NO_2)\sigma(NO_2) = 4.41 \pm 0.08$ (error is 2σ from the fit).

cence signal by I_2) and NO_2 respectively; $\Phi^{O^3P}_{355\ nm}(IO)$ and $\Phi^{O^3P}_{355\ nm}(NO_2)$ are the quantum yields of O(^{3}P) for IO and NO_2 photolysis at 355 nm, respectively. $\sigma_{355\ nm}(IO)$ and $\sigma_{355\ nm}(NO_2)$ are the absorption cross sections of IO and NO_2 at 355 nm, respectively. There is no term in eq ii for laser fluence since, within measurement uncertainty, the fluence was unchanged for both IO and NO_2 photolysis. Figure 6 shows the expected linear relationship between $S_o(IO)_{corr}/S_o(NO_2)$ and $[IO]/[NO_2]$, and we obtain a value of $\Phi^{O^3P}_{355\ nm}(IO)\ \sigma_{355\ nm}(IO)/\Phi^{O^3P}_{355\ nm}\ \sigma_{355\ nm}(NO_2) = 4.41 \pm 0.65$. The quoted uncertainty reflects the combined uncertainties of the weighted fit (95% confidence) in Figure 6, where the errors in relative O(^{3}P) signals are the 95% confidence limits from the exponential fits to the O(^{3}P) decays and include an assessment of systematic errors in [IO] (14% in $\sigma(IO)_{427.2\ nm}$) and $[NO_2]$ (4%). As diagnostic tests, we showed there was no systematic dependence of the slope of Figure 6 on 355-nm laser fluence (≈ 8−30 mJ cm^{-2}), 248-nm laser fluence (≈30−60 mJ cm^{-2}), or the initial concentration of IO in the range $(1-5) \times 10^{12}$ cm^{-3}. The intercept in Figure 6 is close to zero, which provides further indication that we are free from chemical and optical interference under the experimental conditions employed and over the time period of the measurements (<4 ms).

By use of $\Phi^{O^3P}_{355\ nm}(NO_2) = 0.986$,[25] $\sigma_{355\ nm}(NO_2) = 4.70 \times 10^{-19}$ cm^2 [25] and $\sigma_{355\ nm}(IO) = 2.25 \times 10^{-18}$ cm^2,[28] we obtain a value of $\Phi^{O^3P}_{355\ nm}(IO) = 0.91 \pm 0.19$. The quoted uncertainty is obtained by including the uncertainties in $\sigma_{355\ nm}(IO)$ (14% systematic error) and $\sigma_{355\ nm}(NO_2)$ (4%) as above. Over each back-to-back experiment, the average respective laser fluences were stable to a few percent. We measured the [IO]−time profiles by absorption spectroscopy in the same laser cross sectional area as used for the RF measurements, and on the time scales employed (<4 ms), diffusion is negligible. We do consider the divergence of the excimer beam over the 1.25 m cell path length when measuring [IO]−time profiles as a systematic error. This will lead to a small concentration gradient of IO through the cell and cause us to underestimate the true [IO] in the RF detection zone. We make a conservative estimate that this effect will be less than 20% and therefore prefer to quote $\Phi^{O^3P}_{355\ nm}(IO)$ as $0.91 \pm {}^{0.19}_{0.26}$ to reflect this uncertainty. The measured quantum yield is close to unity, as expected.

When calculating the atmospheric lifetime of IO with respect to photolysis, it is assumed that the quantum yield is unity throughout its absorption (≈340−480 nm). As far as we are aware, this work represents the first experimental confirmation of a quantum yield close to unity for the production of O(^{3}P) from IO photolysis at any point in its absorption spectrum.

3.3. Formation, Reaction, and Spectrum of OIO. In a set of preparatory experiments, the IO self-reaction was initiated as described above, and the OIO product was detected by absorption spectroscopy using a gated diode array. Measurements were made over the wavelength range 480−650 nm and were comprised of the coaddition of 5000 laser pulses (repetition rate 0.8 Hz) with light intensity recorded 50 ms before the laser pulse (I_o) and post-photolysis spectra recorded at various delays (at least 60 μs) after the laser pulse (I_f). The initial 60-μs delay after firing the 248-nm laser prevented the detection of fluorescence from the laser wavelength cutoff filter. Absorption was measured over a diode array gate time of between 100 and 500 μs. Figure 7 shows an example of absorbance due to both IO and OIO measured with the diode array. The structured absorption due to OIO in the wavelength range 480−650 nm is clearly visible and is in good agreement with the literature.[11] By use of $\sigma_{549.1\ nm}(OIO) = (3.5 \pm 1.5) \times 10^{-17}$ cm^2,[18] we obtain an average OIO concentration of $(9.1 \pm 3.9) \times 10^{11}$ cm^{-3} over the gate open period (700−1200 μs after the 248-nm laser pulse).

We also performed back-to-back time-resolved absorption measurements using the differential absorption due to OIO at the peak of the (5, 1) band (549.1 nm) and the trough between the (5, 1) and the (5, 0) bands (553.0 nm). The results of an experiment in which 2000−4000 laser pulses were averaged is displayed in Figure 8, which shows that OIO reaches a maximum concentration between ≈700−1200 μs after the 248-nm laser pulse. Using the differential cross section of $(2.7 \pm 1.2) \times 10^{-17}$ cm^2,[11,18] we calculate that $[OIO]_{max} = (8.9 \pm 3.8) \times 10^{11}$ cm^{-3}. This value is consistent with the average value obtained above via the diode array over the gate time 700−1200 μs after the laser pulse; Figure 8 shows that the [OIO]−time profile is almost flat over the diode array gate time. This

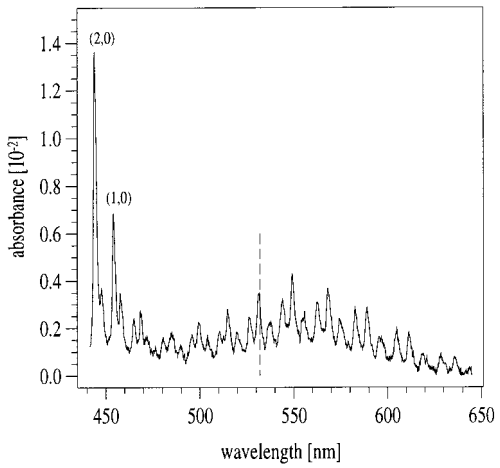

Figure 7. An example of a diode array measurement of the absorption due to a mixture of IO and OIO. The initial [IO] was 5×10^{12} cm^{-3}, and the spectrum was measured over a gate time of 500 μs after an initial delay of 700 μs following the 248-nm excimer laser pulse. 5000 laser pulses were averaged, and the spectrum was been corrected for the change in absorption due to the loss of I_2. The two strong bands on the left of the figure are the (2,0) and (1,0) bands of IO (as labeled), and the structured absorption due to OIO is clearly visible between 480 and 650 nm. The dashed vertical line indicates that our 532-nm photolysis laser is close to the center of the (6,1) band of OIO (assignment from Himmelmann et al.[11]).

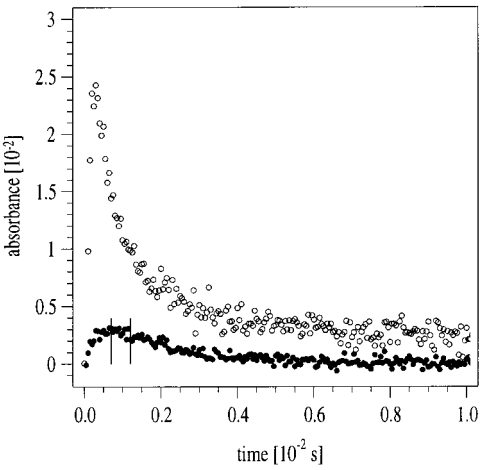

Figure 8. An example of time-resolved absorption and time-resolved differential absorption due to IO (open circles) and OIO (filled circles), respectively. The IO and OIO profiles were obtained by averaging 500 and 2000 laser pulses respectively, each with a time resolution of 50 μs per channel. The initial [IO] was 5×10^{12} cm^{-3}, and the IO and OIO profiles were obtained back-to-back. The vertical lines at $t = 700$ and 1220 μs indicate the gated exposure period of the diode array used to measure the OIO (and IO) absorption features presented in Figure 7.

figure also compares the time characteristics of both IO and OIO and shows that the maximum [OIO] coincides with 30% consumption of IO. These data were employed to optimize the delay between the 248- and 355-nm lasers in the quantum yield measurements in order to ensure maximum [OIO] available for photolysis.

In common with previous spectroscopic studies of OIO generated by the IO self-reaction[11,12] and the IO + BrO reaction,[12] OIO was found to be a transient species, which reached its maximum concentration after ≈1 ms and was lost in ≈5 ms with the initial [IO] at a typical value of 5×10^{12} cm^{-3}. In the present study, we have made no attempt to investigate its loss process(es).

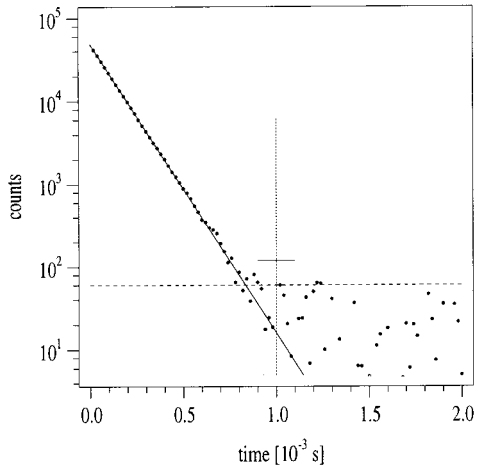

Figure 9. An example of an OIO photolysis experiment; initial [IO] $= 5 \times 10^{12}$ cm^{-3}. Primary O(^{3}P) formed at $t = 0$ in the 248-nm photolysis of O_3 decays by reaction with excess I_2 (solid line is an exponential fit) to form IO. As indicated by the position of the vertical broken line, the 532-nm laser was triggered after a delay of 1 ms (fluence of ≈200 mJ cm^{-2}), at which time $(9 \pm 4) \times 10^{11}$ OIO cm^{-3} was available for photolysis. The top of the vertical broken line is the initial secondary O(^{3}P) signal expected if the quantum yield of OIO is unity at 532 nm. The dashed horizontal line indicates the upper 95% confidence limit of the background signal noise and corresponds to an absolute value of $\approx 8 \times 10^9$ O(^{3}P) cm^{-3}. For comparison, the shorter solid horizontal line corresponds to twice the maximum noise level and indicates the signal which would be expected if $\Phi^{O^3P}_{532\ nm}(OIO) = 0.018$. These data were obtained via the coaddition of 10^4 laser pulses to give a total integration time of 200 ms per channel.

3.4. Photolysis of OIO at 532 nm; Detection of O(^{3}P). With the temporal behavior of OIO established, we performed time-resolved RF experiments under the same experimental conditions as the absorption measurements. We employed the excimer laser at 248 nm to generate IO/OIO and attempted to photolyze the OIO with the Nd:YAG laser at 532 nm and detect the O(^{3}P) product of reaction 10a. The vertical dotted line in Figure 7 is at 532-nm and shows that the 532 nm photolysis beam is situated almost at the head of the (6,1) band of OIO (18813 cm^{-1}).

The methodology was essentially that described above for IO radicals, except we did not employ a reference compound. Quantum yield experiments were performed where we attempted to photolyze OIO at 532 nm ≈1 ms after the 248-nm laser pulse, when OIO has reached its maximum concentration. The 532-nm laser fluence was fixed at ≈27, 56, 122, 156, or 200 mJ cm^{-2}. Even at the highest fluences, we observed no O(^{3}P) signal due to OIO photolysis above our background noise. We also performed experiments where we varied the delay of the 532-nm laser between 1 and 4 ms and observed no secondary O(^{3}P) signal above our noise level. Figure 9 shows an example of these measurements, where we followed the decay of primary O(^{3}P) to completion and then triggered the 532-nm laser (fluence ≈ 200 mJ cm^{-2}) after 1 ms, where maximum [OIO] ($(9 \pm 4) \times 10^{11}$ cm^{-3}) occurs. The horizontal dashed line indicates our absolute detection limit for O(^{3}P) of $(8.0 \pm 1.6) \times 10^9$ cm^{-3} for a 200-ms integration time. If the quantum yield were unity and with $\sigma_{532\ nm}(OIO) = (2.4 \pm 1.0) \times 10^{-17}$ cm^2, we would expect a signal of the magnitude indicated by the top of the dotted vertical line in Figure 9. We can therefore place an upper limit to $\Phi^{O^3P}_{355\ nm}(OIO)$ of 0.009 from these data. Since there are considerable uncertainties in our O(^{3}P) detection limit (±30%), we quote a value of $\Phi^{O^3P}_{532\ nm}(OIO) < 0.012$. Here, we do not consider the potential systematic error induced by the concentra-

tion gradient of OIO along the cell due to excimer beam divergence (see previous section).

Note that the present method used to derive the quantum yield for $O(^3P)$ is independent of the absolute cross section of OIO used. This is because an absolute cross-section (at ≈549 nm) is first used to convert measured OIO optical densities to a concentration, and then an absolute cross section at 532 nm is used to calculate the optical density (due to the same concentration of OIO) at the photolysis laser wavelength (532 nm). With this method, only the relative cross-sections at 532 and 549 nm need be known, and this value should be relatively error-free.

To test for any potential systematic errors associated with our IO source chemistry, we performed experiments with reaction 17 as the IO source. The rate constant for reaction 17[29] is approximately a factor of 30 lower than that for reaction 12,[25] which necessitated higher CF_3I concentrations than I_2 so that the IO radical and OIO production were of a similar rate. Typically, $(1-3) \times 10^{15}$ cm^{-3} CF_3I was used.

$$O(^3P) + CF_3I \rightarrow IO + CF_3 \qquad (17)$$

With the same $[O_3]$ as above and CF_3I in the range $(1-3) \times 10^{15}$ cm^{-3}, it was possible to generate 5×10^{12} IO cm^{-3} such that the OIO formation and loss kinetics were essentially the same as those described above for the I_2 system (see Figures 7 and 8). OIO was confirmed as a product of reaction 4a as described above. Under these conditions, there was no indication of aerosol formation, and there was no $O(^3P)$ production from 532-nm photolysis of O_3 that remained after the 248-nm laser pulse.

Quantum yield experiments were performed at the same [OIO] and laser fluences employed above and again we observed no secondary $O(^3P)$ signal above our noise level; we put an upper limit to $\Phi^{O^3P}_{532\ nm}(OIO) < 0.005$ from these data. On consideration of the systematic errors described above, we quote a final value of $\Phi^{O^3P}_{532\ nm}(OIO) < 0.007$, which is consistent with the value of $\Phi^{O^3P}_{532\ nm}(OIO) < 0.0012$ obtained by employing reaction 14 as a source of IO radicals. The upper limit obtained in this system is lower than that obtained using reaction 14 as an IO source due to use of a longer integration time. We therefore quote a final upper limit as $\Phi(OIO)_{532\ nm} < 0.007$.

A potential explanation for the inability to observe $O(^3P)$ in the photolysis of OIO is that the laser photolysis wavelength is not coincident with a strong absorption band in the OIO spectrum but lies in a trough between two unresolved rotational lines within the (6,0) band. For this reason, we performed the following experiments to confirm that OIO absorbs at the 532-nm emission provided by the 2nd harmonic of the pulsed Nd:YAG. Using reaction 14 as IO source, we measured time-resolved OIO profiles using both the halogen lamp and the CW-2ω Nd:YAG as analysis light sources. As shown in Figure 10, there is good agreement between differential OIO absorption profiles obtained with the CW 2ω Nd:YAG laser (near the center of the (6, 1) band, 532 nm) in combination with the halogen lamp (valley between the (5, 1) and the (5, 0) bands, 553.0 nm open circles) and with the halogen lamp alone at the same wavelengths (filled squares). The profile obtained with the CW, 2ω Nd:YAG laser has been scaled by a factor of 1.15 to fit the halogen lamp data, thus indicating that the true OIO cross section at the 532-nm wavelength of the pulsed Nd:YAG laser is only slightly lower than the cross section employed in the quantum yield study described below but is well within the quoted error limit. The same result was obtained with reaction 17 as the IO source.

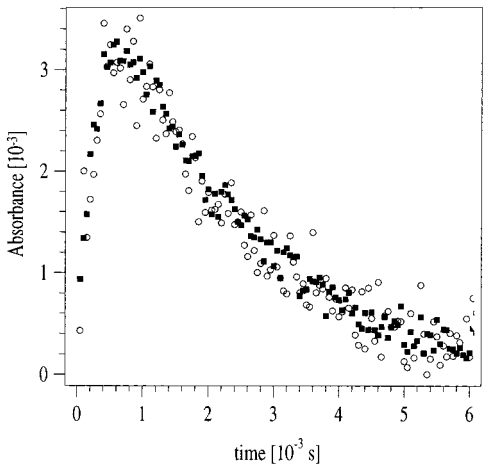

Figure 10. A comparison of differential OIO absorption profiles (described in the text) where (i) the CW 2ω Nd:YAG laser was employed together with the halogen lamp (open circles; scaled by a factor of 1.15 to fit the filled square data) and (ii) by use of the halogen lamp alone (filled squares). IO radicals were generated by reaction 12 such that [OIO] reached a maximum of $(9 \pm 4) \times 10^{11}$ cm^{-3} after ≈1 ms. In both cases, 2000 laser pulses were averaged, each with a time resolution of 50 μs to obtain the absorption profile at each selected wavelength.

For the analysis, we have chosen until now to quote cross sections of OIO based on the work of Himmelmann et al.[11] and Spietz et al.,[18] rather than the value cited by Cox et al.[12] By inspection of Figure 8, it is possible to show that the *differential* cross section of OIO between 549.1 and 553 nm cannot be lower than 1.8×10^{-17} cm^2. This is obtained by assuming 100% yield for OIO formation in the IO self-reaction, (i.e., at $t = 1 \times 10^{-3}$ s, 50% of the IO (≈2.5×10^{12} cm^{-3}) has reacted and the maximum concentration of OIO is 1.25×10^{12} cm^{-3}) and ignores loss processes of OIO, which are clearly present. This results in a very conservative minimum cross section at 548.6 nm of ≈2.7×10^{-17} cm^2, which is considerably higher than the value reported by Cox et al.[12] If we assume a yield of ≈50% for OIO formation from the IO self-reaction, the cross section at 548.6 nm, would have to be doubled.

3.5. Photolysis of OIO at 532 nm; Detection of I. Once it had been established that the photodissociation of OIO to form $O(^3P)$ was inefficient, the alternative photolysis channel leading to the formation of O_2 and $I(^2P_J)$ was investigated. This process is endothermic by 30.1 ± 15.0 kJ mol^{-1} if one considers the electronic ground-state $I(^2P_{3/2})$, which leads to a thermodynamic photodissociation threshold in the mid-IR. This process may be favorable in terms of overall thermochemistry but may involve a significant barrier, as the excited state will require restricted geometry for this decomposition channel. However, the 532-nm photolysis light employed here excites the OIO into the (6, 1) (ν'_1 = I−O stretch, ν'_2 = I−O−I angle bend) level of the $\tilde{A}$ state, such that there is one quanta in the I−O−I angle bending vibration, which may facilitate dissociation via channel (10b):

$$OIO + h\nu \rightarrow I(^2P_J) + O_2 \qquad (10b)$$

Experiments were therefore carried out in which the RF part of the experiment was modified for the detection of $I(^2P_J)$ (see Experimental Section). For experiments in which $I(^2P_J)$ is to be detected, the previous methods of generation of IO by 248-nm photolysis of O_3 in the presence of I_2 or CF_3I are unsuitable, as they generate large amounts of $I(^2P_J)$ either via the reaction of $O(^3P)$ with I_2 (reaction 14) or by CF_3I photolysis:

$$CF_3I + h\nu\ (248\ nm) \rightarrow CF_3 + I \qquad (18)$$

For this reason, the experiments were carried out using the excimer laser photolysis of CH_2I_2 at 351 nm in the presence of O_3; typically the initial concentration of CH_2I_2 was 1×10^{14} cm^{-3}.

$$CH_2I_2 + h\nu\ (351\ nm) \rightarrow CH_2I + I \qquad (19)$$

$$I + O_3 \rightarrow IO + O_2 \qquad (1)$$

Generally, an ozone concentration of $(4-8) \times 10^{15}$ cm^{-3} was added to the system to ensure than $I(^2P_J)$ was converted rapidly to IO. The self-reaction of IO and the formation of OIO could then be followed by time-resolved absorption spectroscopy, as described above. The OIO and IO profiles were similar to those already presented, although in this case, the maximum OIO concentration was reached after $\approx 2-3$ ms instead of after 1 ms when $O(^3P) + I_2$ or $O(^3P) + CF_3I$ were used to make IO. The 532-nm laser was triggered at various delays after the 351-nm laser. A typical primary I signal (from CH_2I_2 photolysis) and a secondary I signal from OIO photolysis at 532 nm ($\approx$100 mJ/cm^2) at time = 0.5 ms are displayed in Figure 11. Note that the decay of $I(^2P_J)$ is not strictly exponential, which is due to its reformation in the IO self-reaction, channels 8a and 8c.

Control experiments revealed that a small RF signal was also obtained when the 351-nm laser (which generates the IO and OIO) was disabled (lower curve in Figure 11). The portion of this signal at $t > 8$ ms decays at a rate consistent with the reaction of $I(^2P_J)$ with O_3 and is due to the 532-nm photolysis of a small I_2 impurity in the CH_2I_2 sample. The rise at shorter times is thought to be associated with the dissociation of O_3 at 532 nm in the Chappuis band to form $O(^3P)$, which can react with I_2 and possibly CH_2I_2 to form I. The size of the correction was $\approx$15% of the total secondary I signal if the timing of the 532-nm laser was adjusted to coincide with the maximum concentration of OIO. Preliminary measurements using laser-induced fluorescence detection also revealed the formation of I_2, either directly in the self-reaction of IO or in subsequent secondary chemistry. The presence of I_2 also represents a further channel for formation of $I(^2P_J)$ following 532 nm irradiation, though we note that the absorption cross section of I_2 at 532-nm ($\approx 3.1 \times 10^{-18}$ cm^2)[27] is approximately an order of magnitude less than that of OIO and the quantum yield for $I(^2P_J)$ formation is less than unity, [30] which reduces the significance of a potential contribution to the measured $I(^2P_J)$ signal.

Our results indicate that, in contrast to $O(^3P)$, $I(^2P_J)$ can be formed from OIO photolysis at this wavelength. To check that OIO is the photolytic precursor to $I(^2P_J)$ in these experiments, the delay between the 351- and 532-nm lasers was varied between 1 and 20 ms to map out the OIO profile. The results of this are displayed in Figure 12, where the $I(^2P_J)$ signal has been extrapolated back to the time of the 532-nm laser pulse. The good agreement in the shape of the $I(^2P_J)$ signal and the OIO profile are taken as confirmation that OIO is the photolytic precursor of the $I(^2P_J)$ atoms rather than I_2, which would be expected not to react further in this system but to reach a plateau as the IO self-reaction approaches completion.

In a further set of experiments we varied the 532-nm laser fluence, with all other parameters held constant. The $I(^2P_J)$ signals displayed a roughly linear dependence on the laser fluence between $\approx$90 and 140 mJ/cm^2. Calculations showed, however, that with a combination of these high laser fluences and the large cross sections of OIO at 532 nm, the transition should be saturated, and there should be no dependence of I

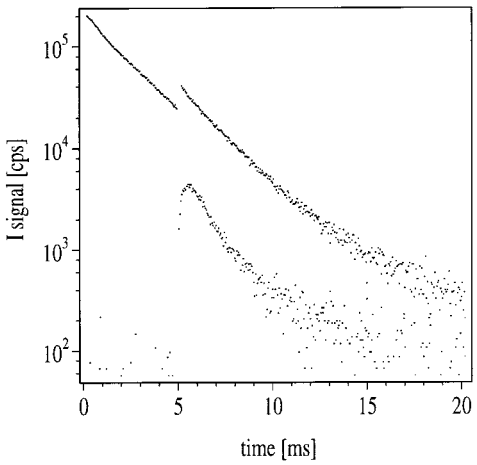

Figure 11. Upper curve: formation and reaction of primary I ($t < 5$ ms) formed in the 351-nm photolysis of CH_2I_2 in the presence of O_3 and secondary I ($t < 5$ ms) formed in the subsequent photolysis of OIO at 532 nm. The laser fluences were 150 mJ cm^{-2} at 351 nm and 90 mJ cm^{-2} at 532 nm. The concentrations of reactants were $[O_3] = 3.8 \times 10^{14}$ cm^{-3} and $[CH_2I_2] = 1.1 \times 10^{14}$ cm^{-3}. The lower curve is that obtained when the 351-nm laser was disabled. The experiments were carried out at a total pressure of 60 Torr N_2.

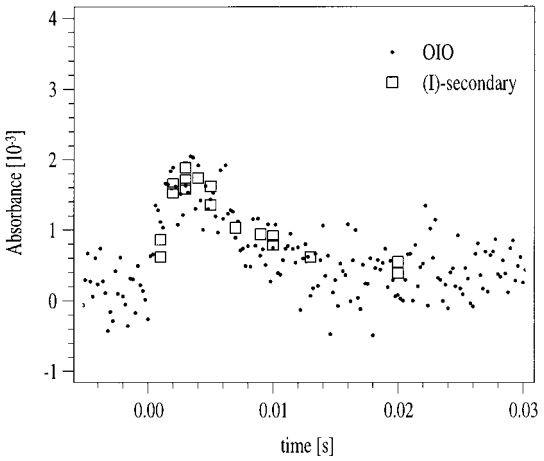

Figure 12. Secondary I signal (open squares) from 532-nm photolysis of OIO as a function of time after the 351-nm excimer laser pulse. Also shown is the OIO profile (dots) obtained under the same experimental conditions. The concentrations of reactants were as given in Figure 11.

yield on laser fluence if this is a single photon process. We therefore interpret the observations at higher fluences as due to dissociation via a sequential two-photon absorption, with saturation of the first transition. When laser fluences of $\approx$2 mJ/cm^2 were used, the $I(^2P_J)$ signal was no longer observable, even though at these "low" fluences, >10% of the OIO, that is, $\approx 5 \times 10^{10}$ cm^{-3} OIO, would have been promoted to an excited state, and that a signal due to $I(^2P_J)$ would have been easily observable if this state was dissociative, with a unity quantum yield to give $I(^2P_J)$ and O_2.

In a manner similar to the experiments used to determine the quantum yield of $O(^3P)$ formation from OIO at 532 nm, the inability to observe of $I(^2P_J)$ at the lower fluences allows us to place an upper limit on the quantum yield for $I(^2P_J)$ formation in a single photon process. In this case, the best measurement of the upper limit is $\Phi^{I}_{532\ nm}(OIO) < 0.1$. Despite similar detection limits for $O(^3P)$ and I, this upper limit is considerably higher than that for $\Phi^{O(^3P)}_{532\ nm}(OIO)$ for a number of reasons. First, the use of an excess concentration of O_3 to generate IO

from the reaction of $I(^2P_J) + O_3$ means that the signal due to primary I never decays to zero over the time scale for which OIO is present (cf. Figures 3 and 11). This is due to the regeneration of $I(^2P_J)$ in the IO self-reaction. Even if very large O_3 concentrations were employed, a substantial primary I signal remained at the time the 532-nm laser was triggered, precluding detection of a small additional secondary I signal. Note that for the $O(^3P)$ experiments, the primary $O(^3P)$ signal decayed to 2.5 ‰ of its original signal by the time the OIO concentration was maximized at ≈1 ms. This observation effectively rules out the presence of an $O(^3P)$-forming channel in the IO self-reaction, that is,

$$IO + IO \rightarrow I_2O + O(^3P) \quad (8e)$$

This ideal situation could never be reached in the $I(^2P_J)$ experiments, where the primary I signal only decayed to 2−4% of its initial value by the time the OIO signal had maximized and the 532-nm laser was triggered.

Second, I_2, which is both present as an impurity in the CH_2I_2 sample and formed either in a minor channel of the IO self-reaction or in secondary chemistry, is dissociated by the 532-nm laser pulse to form I. Although the formation of $I(^2P_J)$ in the photolysis of impurity I_2 can be easily corrected as described in the text, a simple correction is not possible for the photolysis of I_2 generated in this chemical system, as its yield has not been accurately established. These factors, combined with errors associated with the calibration of the $I(^2P_J)$ signal, lead us to place a final upper limit of ≈0.15 on $\Phi^{O^3P}_{532\ nm}(OIO)$.

3.6. Atmospheric Implications. As far as we are aware, this work represents the first experimental study of the photochemistry of OIO. We have been unable to detect either $O(^3P)$ or $I(^2P_J)$ from the photolysis of OIO in a single photon process within its visible absorption manifold at 532 nm. Our results are restricted to 532 nm, and clearly, more studies are required with tuneable photolysis sources to assess the possibility of dissociation from the other (ν'_1, ν'_2) levels of the OIO $\tilde{A}$ state. However, we initially assume that the present result is applicable to the whole of the visible absorption of OIO. The result for $O(^3P)$ corroborates the predictions by ab initio calculations,[19] and the atmospheric fate of OIO will not be determined by photolysis, forming $O(^3P)$. Although we were unable to detect the production of $I(^2P_J)$ in the 532-nm photolysis of OIO, our upper limit for this process is very high, and we note that a quantum yield of 0.15 would be sufficient to make photolysis to O_2 and $I(^2P_J)$ the dominant loss process for OIO in the atmosphere. By comparison with OClO, where ejection of the central halogen atom by photolysis is inefficient, we expect that the same might apply to OIO. In the following, we examine some of the potential reactions of OIO that, in the absence of a photolytic removal process, may be important.

Of the reactions with trace species, the exothermic processes shown below are expected to occur; all thermochemical data were taken from ref 25 except $\Delta H_f(HOI) = -64.9 \pm 5.4$[19] and $\Delta H_f(IO) = 115.9 \pm 5.0$ kJ mol^{-1}.[20]

$$OH + OIO \rightarrow HOI + O_2 \qquad \Delta H_r = -180.5 \pm 15.9 \text{ kJ mol}^{-1} \quad (20)$$

$$NO + OIO \rightarrow NO_2 + IO \qquad \Delta H_r = -18.0 \pm 15.8 \text{ kJ mol}^{-1} \quad (21)$$

Reactions 20 and 21 are assumed to occur by analogy with the OClO reactions 22 and 23 and the OBrO reaction 24, respectively, where $k_{22} = 6.8 \times 10^{-12}$,[25] $k_{23} = 3.4 \times 10^{-13}$ cm^3 s^{-1},[25] and $k_{24} = 1.8 \times 10^{-12}$ cm^3 s^{-1} [32] at 298 K:

$$OH + OClO \rightarrow HOCl + O_2 \qquad \Delta H_r = -208.8 \pm 13.2 \text{ kJ mol}^{-1} \quad (22)$$

$$NO + OClO \rightarrow NO_2 + ClO \qquad \Delta H_r = -35.8 \pm 6.3 \text{ kJ mol}^{-1} \quad (23)$$

$$NO + OBrO \rightarrow NO_2 + BrO \quad (24)$$

In addition, transfer to the aerosol phase is a potentially important loss process. Observations of a large enrichment of the I/Cl ratio in marine aerosol, which is typically 100−1000 times the seawater ratio[33] are presently not fully explained but may involve the scavenging of gas-phase organic or inorganic iodine by the longer-lived small particles. The short lifetime of the inorganic iodine reservoir species HOI and $IONO_2$ with respect to photolysis may limit the effectiveness of heterogeneous scavenging, whereas the potentially long lifetime of OIO with respect to photolysis makes it a good candidate for scavenging.

4. Conclusions

The transient species IO and OIO were generated in situ via pulsed laser photolysis, and their concentration−time profiles were characterized by time-resolved UV−visible absorption spectroscopic techniques. Photofragment spectroscopy was employed to investigate the $O(^3P)$ quantum yield for each species following photolysis at either 355 or 532 nm. The quantum yield for OIO was found to be <0.007 for excitation to the (6, 1) level of the $\tilde{A}$ state at 532 nm. The quantum yield for formation of $O(^3P)$ in the 355-nm photolysis of the IO radical at 355 nm was determined as $0.91 \pm {}^{0.19}_{0.26}$. $I(^2P_J)$ could not be detected in the single photon photolysis of OIO at 532 nm, and an upper limit of ≈0.15 for the quantum yield for the process could be determined.

References and Notes

(1) Vogt, R.; Sander, R.; von Glasow, R.; Crutzen, P. J. *J. Atmos. Chem.* **1999**, *32*, 375.
(2) Chameides, W. L.; Davis, D. D. *J. Geophys. Res.* **1980**, *85*, 7383.
(3) Chatfield, R. B.; Crutzen, P. J. *J. Geophys. Res.* **1990**, *95*, 22319.
(4) Davis, D.; Crawford, J.; Liu, S.; McKeen, S.; Bandy, A.; Thornton, D.; Rowland, F.; Blake, D. *J. Geophys. Res.* **1996**, *101*, 2135.
(5) Jenkin, M. E.; Cox, R. A.; Candeland, D. E. *J. Atmos. Chem.* **1985**, *2*, 359.
(6) Jenkin, M. E. A comparative assessment of the role of iodine photochemistry in tropospheric ozone depletion. In *The Tropospheric Chemistry of Ozone in the Polar Regions*; NATO ASI Series; Niki, H., Becker, K. H., Eds.; Springer-Verlag: Berlin Heidelberg, 1993; Vol. I7.
(7) Roehl, C. M.; Burkholder, J. B.; Moortgat, G. K.; Ravishankara, A. R.; Crutzen, P. J. *J. Geophys. Res.* **1997**, *102*, 12819.
(8) Stutz, J.; Hebestreit, K.; Alicke, B.; Platt, U. *J. Atmos. Chem.* **1999**, *34*, 65.
(9) Carpenter, L. J.; Sturges, W. T.; Penkett, S. A.; Liss, P. S.; Alicke, B.; Hebestreit, K.; Platt, U. *J. Geophys. Res.* **1999**, *104*, 1679.
(10) Bauer, D.; Ingham, T.; Carl, S. A.; Moortgat, G. K.; Crowley, J. N. *J. Phys. Chem.* **1998**, *102*, 2857.
(11) Himmelmann, S.; Orphal, J.; Bovensmann, H.; Richter, A.; Ladstätter-Weissenmayer, A.; Burrows, J. P. *Chem. Phys. Lett.* **1996**, *251*, 330.
(12) Cox, R. A.; Bloss, W. J.; Jones, R. L.; Rowley, D. M. *Geophys. Res. Lett.* **1999**, *26*, 1857.
(13) Sander, R.; Crutzen, P. J. *J. Geophys. Res.* **1996**, *101*, 9121.
(14) Vogt, R.; Crutzen, P. J.; Sander, R. *Nature* **1996**, *383*, 327.
(15) Ayers, G. P.; Gillett, R. W.; Cainey, J. M.; Dick, A. L. *J. Atmos. Chem.* **1999**, *33*, 299.
(16) Fickert, S.; Adams, J. W.; Crowley, J. N. *J. Geophys. Res.* **1999**, *104*, 23719.

(17) Bedjanian, Y.; Le Bras, G.; Poulet, G. *J. Phys. Chem.* **1998**, *102*, 10501.

(18) Spietz, P.; Himmelmann, S.; Gross, U.; Bleck-Neuhaus, J.; Burrows, J. P. A complex approach to investigate the chemistry and kinetics of IOx using flash photolysis and time-resolved absorption spectroscopy. 15th Int. Symp. Gas Kinetics, Bilbao, Spain, 1998.

(19) Misra, A.; Marshall, P. *J. Phys. Chem.* **1998**, *102*, 9056.

(20) Bedjanian, Y.; Le Bras, G.; Poulet, G. *J. Phys. Chem.* **1997**, *101*, 4088.

(21) Ingham, T.; Bauer, D.; Sander, R.; Crutzen, P. J.; Crowley, J. *J. Phys. Chem.* **1999**, *103*, 7199.

(22) Ingham, T.; Bauer, D.; Landgraf, J.; Crowley, J. N. *J. Phys. Chem.* **1998**, *102*, 3293.

(23) Deakin, J. J.; Husain, D. *J. Chem. Soc., Faraday Trans.* **1972**, *68*, 1603.

(24) Donovan, R. J.; Husain, D. *Trans. Faraday Soc.* **1966**, *62*, 2023.

(25) DeMore, W. B.; Sander, S. P.; Golden, D. M.; Hampson, R. F.; Kurylo, M. J.; Howard, C. J.; Ravishankara, A. R.; Kolb, C. E.; Molina, M. J. *Chemical Kinetics and Photochemical Data for Use in Stratospheric Modelling*; No. 11; Jet Propulsion Laboratory, 1997.

(26) Schneider, W.; Moortgat, G. K.; Tyndall, G. S.; Burrows, J. P. *J. Photochem. Photobiol.* **1987**, *40*, 195.

(27) Tellinghausen, J. *J. Chem. Phys.* **1973**, *58*, 2821.

(28) Harwood, M. H.; Burkholder, J. B.; Hunter, M.; Fox, R. W.; Ravishankara, A. R. *J. Phys. Chem. A* **1997**, *101*, 853.

(29) Gilles, M. K.; Turnipseed, A. A.; Talukdar, R. K.; Rudich, Y.; Villalta, P. W.; Huey, L. G.; Burkholder, J. B.; Ravishankara, A. R. *J. Phys. Chem.* **1996**, *100*, 14005.

(30) Okabe, H. *Photochemistry of Small Molecules*; Wiley: New York, 1978.

(31) Donovan, R. J.; Hathorn, F. G. M.; Husain, D. *Trans. Faraday Soc.* **1968**, *64*, 3192.

(32) Li, Z. J.; Tao, Z. N. *Chem. Phys. Lett.* **1999**, *306*, 117.

(33) Moyers, J. L.; Duce, R. A. *J. Geophys. Res.* **1972**, *77*, 5229.